Journal of Magnetic Resonance 200 (2009) 142–146

Contents lists available at ScienceDirect

Journal of Magnetic Resonance

journal homepage: www.elsevier.com/locate/jmr

Communication

# Nearly $10^6$-fold enhancements in intermolecular $^1$H double-quantum NMR experiments by nuclear hyperpolarization

Mor Mishkovsky [a], Uzi Eliav [b,*], Gil Navon [b], Lucio Frydman [a,*]

[a] Chemical Physics Department, Weizmann Institute, 76100 Rehovot, Israel
[b] School of Chemistry, Tel Aviv University, 69978 Tel Aviv, Israel

ARTICLE INFO

*Article history:*
Received 26 February 2009
Revised 28 May 2009
Available online 6 June 2009

*Keywords:*
Intermolecular multiple-quantum coherences
Nuclear hyperpolarization
Double-quantum NMR
DNP
EPI MRI

ABSTRACT

Intermolecular Multiple-Quantum Coherences (iMQCs) can yield interesting NMR information of high potential usefulness in spectroscopy and imaging – provided their associated sensitivity limitations can be overcome. A recent study demonstrated that *ex situ* dynamic nuclear polarization (DNP) could assist in overcoming sensitivity problems for iMQC-based experiments on $^{13}$C nuclei. In the present work we show that a similar approach is possible when targeting the protons of a hyperpolarized solvent. It was found that although the DNP procedure enhances single-quantum $^1$H signals by about 600, which is significantly less than in optimized low-$\gamma$ liquid-state counterparts, the non-linear dependence of iMQC-derived signals on polarization can yield very large enhancements approaching $10^6$. Cleary no practical amount of data averaging can match this kind of sensitivity gains. The fact that DNP endows iMQC-based $^1$H NMR spectra with a sensitivity that amply exceeds that of their thermally polarized single-quantum counterpart, is confirmed in a number of simple single-scan 2D imaging experiments.



## 1. Introduction

Intermolecular multiple quantum coherences (iMQCs [1–4]) can provide a valuable contrast in both NMR spectroscopy and imaging (MRI) [5–17]. This is the result of iMQCs' peculiar dependence on inter-spin distances, typically in the order of 0.05–1 mm, of their dependence on the medium's mesoscopic morphological and susceptibility properties, and of their non-linear variation with the size of the magnetization. These features have led to a number of alternative approaches for exciting iMQC states, and to numerous ways of monitoring their consequences on different NMR and MRI experiments [1–17]. The basic iMQC pulse sequence relies on the CRAZED scheme initially proposed by Warren and coworkers [1], whereby non-linear elements in the density matrix are excited and allowed to generate observable single-quantum signals with the aid of suitably set magnetization gratings:

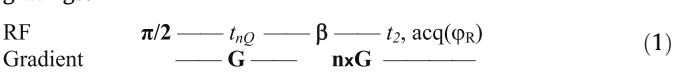


(1)

Here $n$ is the order of the selected quantum coherence, $t_{nQ}$ is the evolution time of this $n$th coherence, and $G$ is a gradient that – when combined with a suitable radiofrequency (RF) pulse of tilt angle $\beta$ – will generate a longitudinal magnetization grating that converts these non-linear terms into detectable signals. The rate $1/\tau_D$ characterizing this conversion is in turn given by $(3\cos^2\theta - 1)\gamma^2\mu_0\hbar NP\sin\beta$, where $P$ is the polarization and $N$ the particle number in the intervening spin ensemble, and $\theta$ is the orientation of field gradient with the magnetic field. Neglecting diffusion and longitudinal relaxation effects the time-domain signal observed as a function of $t_2$ in this kind of iMQC experiments is then given by [1,2,13,14]:

$$S(t_2) = \gamma\hbar NPi^{n-1}\{[n\tau_D J_n(t_2/\tau_D)/t_2 - 1/2[J_{n-1}(t_2/\tau_D) - J_{n+1}(t_2/\tau_D)]\cos\beta]\}exp(-t_2/T_2^*) \quad (2)$$

where the $\{J_n\}$ represent the Bessel functions corresponding to the selected coherence, $T_2$ is the usual transverse relaxation time, and $i = \sqrt{-1}$. For the $n = 2$ state relevant in this study and $T_2^*/\tau_D \leqslant 1$ this expression can be further simplified to:

$$S(t_2) = i[3\cos^2\theta - 1]\gamma\mu_0(\gamma NP\hbar)^2 t_2 \sin\beta(1 - \cos\beta)exp(-t_2/T_2^*)/4 \quad (3)$$

In the current study, the dependence of the spectral intensity on polarization $P$ was studied by measuring the peak height of the iDQC signal following its Fourier transform. An analytical expression for this height can be obtained by Fourier transformation of Eq. 3; taking the conditions in the current study for $\beta = 60°$, $\theta = 0°$ the expression for the peak height is [18]:

$$S^{max} = \gamma^3\mu_0(NP\hbar T_2^*)^2\sqrt{3}/16 \quad (4)$$

* Corresponding authors.
*E-mail addresses:* eliav@post.tau.ac.il (U. Eliav), lucio.frydman@weizmann.ac.il (L. Frydman).

1090-7807/$ - see front matter © 2009 Elsevier Inc. All rights reserved.
doi:10.1016/j.jmr.2009.06.002

This quadratic dependence of the iDQC spectral amplitudes on $N$, $P$ and $T_2^*$, can be shown by numerical means to hold valid for $T_2^*/\tau_D < 3$. This dependence highlights one of the main handicaps facing experiments exploiting these states, as it suggests that for spin systems possessing small equilibrium magnetizations, iMQC-oriented experiments will be progressively less sensitive than their conventional single-pulse counterparts. iDQC-based $^1$H MRI experiments have therefore been extensively documented using abundant components such as water or fat, but are challenging when considering low-concentration metabolites or low-$\gamma$ nuclides.

The last few years have witnessed the appearance and expanded use of analytical hyperpolarization approaches, in which NMR is implemented on spin states whose polarization exceeds by orders of magnitude the usual ppm levels [19–21]. Counted among these methods is dynamic nuclear polarization (DNP), a methodology whereby a target molecule of interest is co-mixed with an electron radical, frozen in a glass under cryogenic conditions, and irradiated at or near the electron's microwave Larmor frequency [21,22]. Under suitable conditions this irradiation can transfer the electron's spin alignment into the nuclear reservoir, and lead to NMR polarizations reaching up to nearly the maximal value of one. In the *ex situ* DNP procedure that will here concern us such cryogenic hyperpolarized states are then ported away from the hyperpolarizing magnet by a sudden dissolution with hot vapors, which carry the sample away into an NMR or MRI scanner for an otherwise conventional liquid-state observation [23,24]. The availability of a commercial instrument capable of performing this kind of DNP-based liquid-state hyperpolarization, has created substantial interest both toward biological investigations as well as in terms of analytical spectroscopy [25–28]. Very recently for example Warren and coworkers showed that this Hypersense® DNP machine makes it possible to detect iMQCs between $^{13}$C nuclei [29], promising to greatly expand the potential scope of these experiments. In the current study we explore the capabilities that may arise from the combined use of this DNP machine, with $^1$H-based NMR and MRI procedures. It is observed that the non-linear dependence of iMQCs on polarization make it possible to enhance the double-quantum signals arising from solvents by factors of ca. $10^6$, thereby enabling a number of otherwise unfeasible single-scan 2D MRI acquisitions.

## 2. Results and discussion

To explore the possibilities arising from $^1$H NMR measurements based on *ex situ* DNP hyperpolarization, we focused on the behavior of the $^1$H double-quantum coherent states of $CD_3OH$. In such system intra-molecular $J$ couplings will not play any significant role, and intermolecular interactions are dominant. Added advantages of $CD_3OH$ over other potential targets such as $CH_3OD$ or HDO included a relatively long $T_1$ under non-degassed conditions (10.8 s), and a relatively efficient hyperpolarization. DNP was performed on a 50% v/v solution of $CD_3OH$ in DMSO-$d_6$; the resulting glass was co-mixed with TEMPO at a 30 mM concentration, and polarized using an OIMBL Hypersene® machine for ca. 15–20′ at 1.5 K to achieve maximal polarization. The targeted molecule was then dissolved and transferred from the 3.35 T DNP system to an 11.7 T NMR magnet using $CD_3OD$ as melting/carrying solvent, resulting in a final $CD_3OH$ concentration of ≈170 mM. It is worth noting that in spite of this ensuing dilution and of eventual proton ↔ deuterium exchanges happening during the transfer and throughout the data acquisition, all observable protons in the resulting solution remain equivalent and homogeneously polarized during the NMR measurement.

In order to obtain a reliable evaluation of the iMQC signal enhancements achievable by the *ex situ* DNP setup, the pulse sequence illustrated in Fig. 1A was used. Following a short settling delay for allowing the sample to stabilize inside the magnet, this sequence executes two consecutive measurements (i) a conventional $^1$H single-quantum single-pulse acquisition with a small (≈2.5°) tilt angle, where linear dependence on the magnetization is expected; (ii) immediately thereafter, an iMQC CRAZED-type sequence of the type shown in Eq. 1, with $\beta = 60^o$ and gradients set to maximize the $n = 2$ double-quantum contribution (see Fig. 1 for further details). Given the small tilt angle used in the SQ pulse and the short delay involved in the ensuing acquisition, we estimate that over 95% of the hyperpolarized longitudinal polarization remained for this second iDQC measurements. Fig. 1B–E illustrate

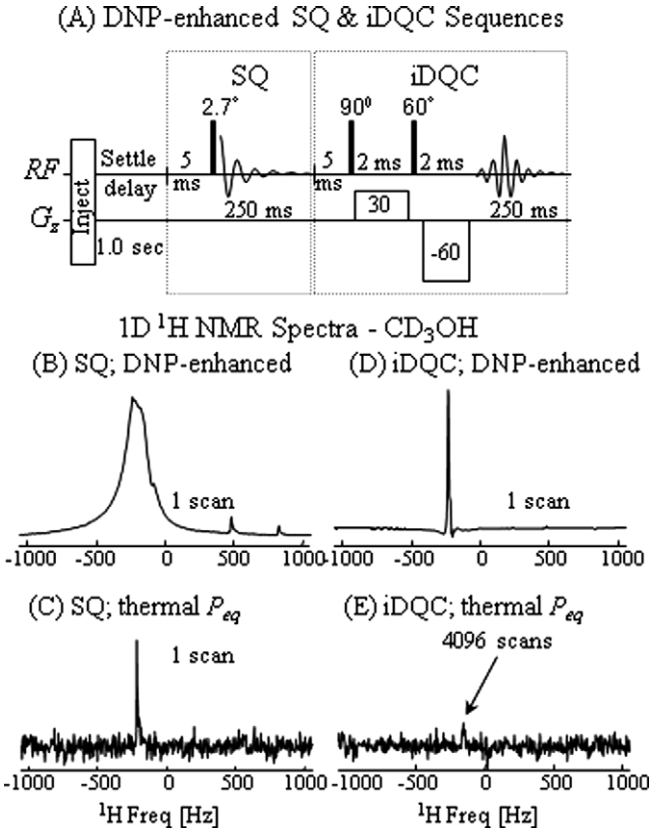


**Fig. 1.** Comparison between SQ and iDQC NMR results obtained on a single $^1$H site, for the same sample under DNP-enhanced and normal thermal polarization conditions. Enhancement was achieved by irradiating for 15–20 min a 30 μL glass made by 30 mM of TEMPO radical dissolved in a $CD_3OH$/DMSO-$d_6$ 50% v/v solution and frozen at 1.5 K, with 50 mW of microwaves centered at 94.2 GHz. Dissolution and transport of the hyperpolarized sample was effected with pressurized (3 bar) $CD_3OD$, leading to a final effective $^1$H concentration of ~0.75% v/v (170 mM) $CD_3OH$. Sequence employed to collect single-scan SQ and iDQC data on the same hyperpolarized solution, showing the pulse angles (°), timings and gradients (in G/cm) involved. Like all remaining experiments in this study, this sequence was implemented on a Varian iNova® 500 MHz NMR spectrometer using a conventional triple-axis 5 mm NMR probe (A) (An attempt to refocus the magnetic field inhomogeneity by inserting a 180° pulse between the 60° pulse and acquisition in the iDQC segment, caused further broadening and lineshape distortion of the spectrum and thus was not considered either in the DNP nor in the thermal equilibrium experiments.). The hyperpolarized $^1$H 1D spectrum arising from the "SQ" segment of the sequence (B) shows a resonance broadened by a combination of magnetic field inhomogeneity (due to air bubbles) and radiation-damping effects. (D) Idem as (B) but for iDQC segment of the experiment. (C) and (E) are as analogous to (B) and (D), but recorded after the sample's magnetization returned to equilibrium. Due to low $S/N$ the iDQC spectrum in (E) could be obtained only after extensive accumulation (4096 scans). Also, in order to avoid spurious SQ signal, an extensive phase cycling was made using a 12 s recycle delay ($T_1$ for the solution used in the DNP and subsequent thermal equilibrium experiments was 3.5 s). The receiver's gain in both thermally polarized experiments (D and E) was raised by 78 dB vis-à-vis their hyperpolarized counterpart acquisitions.

the sensitivity gains achievable by the *ex situ* DNP procedure for these $^1$H SQ and $^1$H iDQC NMR experiments. Whereas the sensitivity of the SQ-based experiments (panels B and C) was sufficient to enable an estimation of the enhancements using the same sample and pulse sequence, the sensitivity of the iDQC experiment under thermal equilibrium was so low that it required extensive signal averaging in order to get minimal reliability in the enhancement calculation. An important factor affecting the enhancement observed in iDQC experiments is $T_2^*$, which as seen in Eqs. 3 and 4 affects spectral intensities in proportion to a second power. Thus an effort was put into shimming the magnetic field so that $T_2^*$(thermal equilibrium)/$T_2^*$(DNP) > 1. Line widths of ca. 7 Hz (i.e., $T_2^* \approx 50$ ms) were obtained for the thermal equilibrium samples. This value is similar to that obtained in the DNP experiments, where $T_2^*$s were evaluated from the decay tail of the FID to be $\leqslant$80 ms. Having $T_2^*$s of similar values for DNP and equilibrium experiments, as well as $T_2^*/\tau_D < 3$, we can conclude on basis of Eqs. 3 and 4, that ratio of peaks heights should provide a good estimate of the signal dependence on the changes in polarization. With these provisions, the signal enhancements afforded by *ex situ* DNP sequences were calculated as $E = (S^{DNP}/N)/(S^{eq}/N)$; here $S$ and $N$ stands for the integral of the peak and the average noise power for the SQ experiment, and for the peak maximum and average noise power intensity for the iDQC case. Factoring in the 4096 scans used in the latter's thermally-polarized acquisition, the data in Fig. 1 reveals that the DNP enhancements arising in the SQ and iDQC experiments are $E \approx 600$ and 730,000, respectively. Due to the low $S/N$ obtained in thermal equilibrium and limited accuracy of $T_2^*$ the latter enhancement value is subjected to a relatively large error, but within this accuracy the iDQC signal conforms to the $P^2$ power dependence predicted by Eqs. 2–4. Moreover, owing to the $P^2$ power dependence, iDQCs experiments carried out on hyperpolarized samples ended up yielding signal intensities that were much closer to those of their single-pulse SQ counterparts, than what happened to be the case under room-temperature polarization conditions. A signal ratio of ~1/8 was thus measured between the iDQC and SQ methods following hyperpolarization, whereas a ratio <1/8000 arose between the two $^1$H experiments when repeated under fully relaxed room-temperature conditions. The second power dependence on the polarization made it difficult to estimate a possible contribution to the signal enhancement from mechanisms [30] other than intermolecular dipolar interaction.

The significant sensitivity increase afforded by DNP, enables the consideration of utilizing such solvent-enhanced signals in $^1$H imaging experiments [31,32]. To investigate this potential a series of 2D $^1$H MRI experiments were carried out on simple phantoms, relying on the single-scan echo-planar-imaging (EPI) sequence [33,34]. As in the spectroscopic examples of Fig. 1, these tests involved the injection of the hyperpolarized sample followed by the acquisition of two consecutive experiments (Fig. 2A). The first of these was a blipped EPI imaging sequence with a non-selective small-angle excitation pulse; the other was an iDQC CRAZED sequence that made use of the remaining magnetization and was followed by EPI. These experiments were executed with a conventional triple-axis gradient 5 mm NMR probe; in the iDQC sequence two of the probe's gradients were employed to implement the gradient-echoed 2D EPI protocol, while the third axis was used to create the intermolecular dipolar gratings and the selection of the desired $0 \rightarrow -2 \rightarrow -1$ coherence transfer pathway. In Fig. 2B–E the transverse $X$–$Y$ plane images arising from such tests are compared. Clearly, the *ex situ* DNP procedure provides once again sufficient SNR to obtain an image whose quality exceeds that is available from a thermally-polarized SQ experiment. Upon comparing the DNP-enhanced *vs.* the thermally-polarized images, the SQ experiment reveals an enhancement of ≈50–100. This constitutes a drop vis-à-vis the hyperpolarization observed

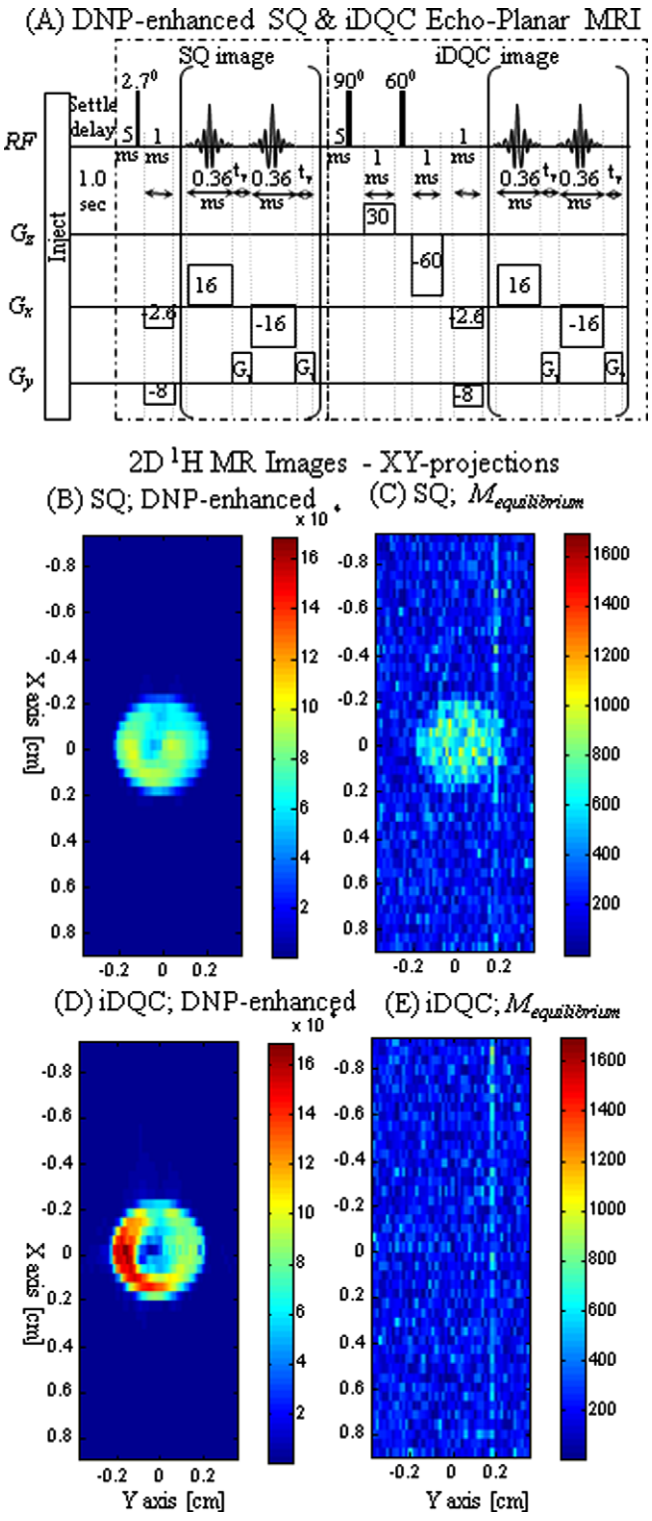


**Fig. 2.** Comparison between SQ and iDQC echo-planar NMR images obtained for the same sample and under similar hyperpolarized/thermal conditions as described in Fig. 1. In this imaging experiment the iDQCs were selected using a $Z$-axis gradient with the indicated parameters, and the EPI images were subsequently measured along the orthogonal $XY$ plane (no $Z$ slice selection). Besides the parameters stated in the sequence (A), additional EPI-related values included $G_y = 1.65$ G/cm and $t_y = 0.1$ ms for the $Y$-axis blips. These data (B–D) were sampled with a time resolution of 8 μs/complex point; following their rearrangement and 2D Fourier transformation the following parameters characterized the images: FOV($X$) = 1.83 cm, $\Delta X = 0.04$ cm, FOV($Y$) = 0.712 cm, $\Delta Y = 0.0148$ cm, matrix size = 45 × 48. Under these conditions no iDQC image could be discerned for a thermally polarized sample, even after extensive signal averaging (E).

in the spectroscopy case, which we presume stems from EPI's higher sensitivity to the inhomogeneity and the broadening conditions present immediately after the Hypersense's sample injection. These will diminish and eventually disappear as the sample rests in the magnet, hence biasing the comparison in favor of the equilibrated experiment. As for the iDQC images – no such estimate could be made due to insufficient sensitivity under thermal equilibrium even after extensive signal averaging. However, from the noise-dominated iDQC EPI images observed after $\geqslant$24 h of signal averaging on this sample, we conclude that DNP enhancements of at least $\approx 10^4$–$10^5$ are once again active in these experiments.

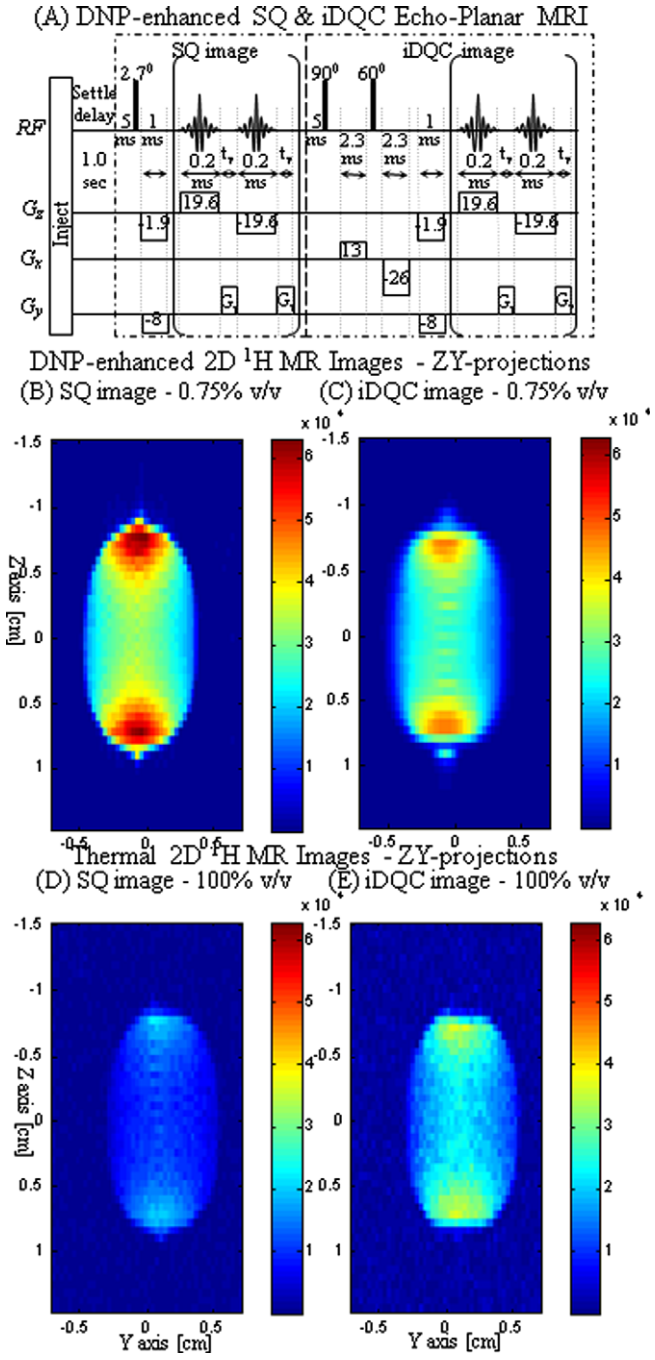


**Fig. 3.** Idem as in Fig. 2, but for longitudinal single-scan EPI experiments where iDQCs were selected using an *X*-axis gradient and EPI images measured along the orthogonal *ZY* plane. Besides all indicated timings and gradients, EPI acquisition parameters included phase-encoding blips $G_y = -1.65$ G/cm, $t_y = 0.1$ ms, FOV($Y$) = 1 cm, $\Delta Y = 0.03$ cm, FOV($Z$) = 3 cm, $\Delta Z = 0.06$ cm, and a $50 \times 48$ final matrix size. The DNP-enhanced iDQC image was measured in a single-scan on 0.75% hyperpolarized $CD_3OH$ (C), whereas the thermal image resulted from a one scan in SQ case (D) and four-scan phase-cycled averaging for the iDQC spectrum (E) were carried out using neat $CD_3OH$ (once again, with a 78 dB difference among their receiver gains). Notice the abrupt ending arising in these two images along the *Z* axis, in comparison to the comparable SQ profiles.

Fig. 3B and C show another comparison between DNP-enhanced SQ and iDQC 2D MRI images, this time obtained for single-scan projections along a longitudinal *Z*–*Y* plane. While these data once again indicate that similar sensitivities characterize the SQ and iDQC imaging experiments, a systematic difference can now be observed between the two sets in the form of a "cropping" of the 2D image along the top and bottom edges of the *Z* axis. This systematic difference was observed repeatedly both for DNP-enhanced experiments, as well as for conventional SQ and multi-scan iDQC acquisitions collected on thermally polarized neat samples (Fig. 3D and E). In all these instances longitudinal profiles that are ca. 3 mm shorter in the iDQC than in SQ images arose; we ascribe these distortions to the higher sensitivity that the iDQC generation and decay processes to $B_1$ and $B_0$ inhomogeneities, as one can expect from Eqs. 2–4, that are more pronounced towards the edges of the coil's field-of-view. Regardless of their precise origin, in the current study these instrumentation-derived imperfections are valuable, as they serve as a source of "contrast mechanism" between the iDQC and SQ imaging experiments. The similarities between the iDQC single-scan image acquired following hyperpolarization and the iDQC thermal equilibrium images collected following phase cycling, further demonstrate that the same double-quantum coherence is being selected in both types of experiments.

## 3. Conclusion

The signal enhancement brought about by *ex situ* DNP makes it possible to execute conventional liquid-state NMR and MRI experiments, at spin concentrations that just would not be practical if one were to rely on thermal equilibrium magnetization. This is particularly true for the case of iMQCs, where sensitivity will in general be limited by the non-linear nature of this phenomenon. The non-linear dependence on the magnetization has been recently exploited for low-$\gamma$ nuclei like $^{13}C$, which can undergo enhancements exceeding 10,000 by *ex situ* DNP. In spite of the ca. 10-fold smaller polarization enhancements imparted by DNP on protons, this preliminary study indicates that also $^1H$-based solvent experiments can benefit from such procedure. Moreover, while it may be true that the $T_1$'s of protons will normally be too short for allowing $^1H$ hyperpolarization to become a routine tool for imaging metabolism, the short build-up times involved in achieving $^1H$ hyperpolarization (usually 5–10′ for the conditions hereby described) could be exploited for repetitive injections. This in turn opens up interesting possibilities of their own, both in terms of imaging applications as well as within spectroscopic settings within the framework of polarization transfer phenomena. This latter phenomenon can enable the observation of metabolites with intrinsic low sensitivity, as well as the detection of molecules that are remotely located from the hyperpolarized material [35]. Some of these features will be further discussed in upcoming studies.

## Acknowledgments

This work was supported by the Israel Science Foundation (ISF 1206/05 (LF) and 1335/07 (GN)), and made possible by the generosity of the Perlman Family Foundation (LF).

## References


[1] W.S. Warren, W. Richter, A.H. Addreotti, B.T. Farmer, Generation of impossible cross-peaks between bulk water and biomolecules in solution NMR, Science 262 (1993) 2005–2009.

[2] S. Lee, W. Richter, S. Vathyam, W.S. Warren, Quantum treatment of the effects of dipole–dipole interactions in liquid nuclear magnetic resonance, J. Chem. Phys. 105 (1996) 874–900.

[3] R. Bowtell, R.M. Bowley, P. Glover, Multiple spin echoes in liquids in a high magnetic field, J. Magn. Reson. 88 (1990) 641–651.

[4] J. Jeener, A. Vlassenbroek, P. Broekaert, Unified derivation of the dipolar field and relaxation terms in the Bloch–Redfield equations of liquid NMR, J. Chem. Phys. 103 (1995) 1309–1332.

[5] W. Richter, S. Lee, W.S. Warren, Q. He, Imaging with intermolecular multiple-quantum coherences in solution-state NMR, Science 267 (1995) 654–657.

[6] W. Richter, M. Richter, W.S. Warren, H. Merkle, P. Andersen, G. Adriany, K. Ugurbil, Functional magnetic resonance imaging with intermolecular multiple-quantum coherences, Magn. Reson. Imaging 18 (2000) 489–494.

[7] L.S. Bouchard, R.R. Rizi, W.S. Warren, Magnetization structure contrast based on intermolecular multiple-quantum coherences, Magn. Reson. Med. 48 (2002) 973–979.

[8] C. Faber, E. Pracht, A. Haase, Resolution enhancement in in vivo NMR spectroscopy: detection of intermolecular zero-quantum coherences, J. Magn. Reson. 161 (2003) 265–274.

[9] J.P. Marques, R. Bowtell, Optimizing the sequence parameters for double-quantum CRAZED imaging, Magn. Reson. Med. 51 (2003) 148–157.

[10] L.S. Bouchard, W.S. Warren, Multiple-quantum vector field imaging by magnetic resonance, J. Magn. Reson. 177 (2005) 9–21.

[11] L.S. Bouchard, F.W. Wehrli, C.L. Chin, W.S. Warren, Structural anisotropy and internal magnetic fields in trabecular bone: coupling solution and solid dipolar interactions, J. Magn. Reson. 176 (2005) 27–36.

[12] W. Barros Jr., J.C. Gore, D.F. Gochberg, Simultaneous measurement of $D$ and $T_2$ using the distant dipolar field, J. Magn. Reson. 178 (2006) 166–169.

[13] W.S. Warren, S. Ahn, The boundary between liquidlike and solidlike behavior in magnetic resonance, J. Chem. Phys. 108 (1998) 1313–1325.

[14] J.H. Zhong, Z. Chen, S.K. Zheng, S.D. Kennedy, Theoretical and experimental characterization of NMR transverse relaxation process related to intermolecular dipolar interactions, Chem. Phys. Lett. 350 (2001) 260–268.

[15] I. Ardelean, R. Kimmich, Diffusion measurements with the pulse gradient non-linear spin echo method, J. Chem. Phys. 112 (2001) 5275–5280.

[16] U. Eliav, G. Navon, Enhancement of magnetization transfer effects by intermolecular multiple quantum filtered NMR, J. Magn. Reson. 190 (2008) 149–153.

[17] W. Ling, U. Eliav, G. Navon, A. Jerschow, Chemical exchange saturation transfer by intermolecular double quantum coherence, J. Magn. Reson. 194 (2008) 29–32.

[18] B. Zheng, Z. Chen, S. Cai, Theoretical formalism and experimental verification of line shapes of NMR intermolecular multiple-quantum coherence spectra, J. Chem. Phys. 123 (2005) 74317(1)–74317(7).

[19] C.R. Bowers, D.P. Weitekamp, Transformation of symmetrization order in nuclear spin magnetization by chemical reaction and nuclear magnetic resonance, Phys. Rev. Lett. 57 (1986) 2645–2648.

[20] M.S. Albert, G.D. Cates, B. Driehuys, W. Happer, B. Saam, C.S. Springer Jr., A. Wishnia, Biological magnetic resonance imaging using laser-polarized $^{129}$Xe, Nature 370 (1994) 199–201.

[21] D.A. Hall, D.G. Maus, G.J. Gerfen, S.J. Inati, L.R. Becerra, F.W. Dahlquist, R.G. Griffin, Polarization-enhanced NMR spectroscopy of biomolecules in frozen solution, Science 276 (1997) 930–932.

[22] A. Abragam, M. Goldman, Nuclear Magnetism: Order and Disorder, Clarendon Press, 1982.

[23] J.H. Ardenkjaer-Larsen, B. Fridlund, A. Gram, G. Hansson, L. Hansson, M.H. Lerche, R. Servin, M. Thaning, K. Golman, Increase in signal-to-noise ratio of >10, 000 times in liquid-state NMR, Proc. Natl. Acad. Sci. USA 100 (2003) 10158–10163.

[24] H. Jóhannesson, S. Macholl, J.H. Ardenkjaer-Larsen, Dynamic nuclear polarization of 1-13C pyruvic acid at 4.6 T, J. Magn. Reson. 197 (2009) 167–175.

[25] K. Golman, R. Zandt, M. Thaning, Real-time metabolic imaging, Proc. Natl. Acad. Sci. USA 103 (2006) 11270–11275.

[26] A.P. Chen, M.J. Albers, C.H. Cunningham, S.J. Kohler, Y.F. Yen, R.E. Hurd, J. Tropp, R. Bok, J.M. Pauly, S.J. Nelson, J. Kurhanewicz, D.B. Vigneron, Hyperpolarized C-13 spectroscopic imaging of the TRAMP mouse at 3 T-initial experience, Magn. Reson. Med. 58 (2007) 1099–1106.

[27] F.A. Gallagher, M.I. Kettunen, S.E. Day, D.-E. Hu, J.H. Ardenkjær-Larsen, R. Zandt, P.R. Jensen, M. Karlsson, K. Golman, M.H. Lerche, K.M. Brindle, Magnetic resonance imaging of pH *in vivo* using hyperpolarized $^{13}$C-labelled bicarbonate, Nature 453 (2008) 940–943.

[28] L. Frydman, D. Blazina, Ultrafast two-dimensional NMR spectroscopy on hyperpolarized solutions, Nat. Phys. 3 (2007) 415–419.

[29] E.R. Jenista, R.T. Branca, W.S. Warren, Hyperpolarized carbon–carbon intermolecular multiple quantum coherences, J. Magn. Reson. 196 (2009) 74–77.

[30] Y.Y. Lin, N. Lisitza, S. Ahn, W.S. Warren, Resurrection of crushed magnetization and chaotic dynamics in solution NMR spectroscopy, Science 290 (2000) 118–121.

[31] R.A. Wind, J.H. Ardenkjær-Larsen, $^1$H DNP at 1.4 T of water-doped with a triarylmethyl-based radical, J. Magn. Reson. 141 (1999) 347–354.

[32] E.R. McCarney, S. Han, Spin-labeled gel for the production of radical-free dynamic nuclear polarization enhanced molecules for NMR spectroscopy and imaging, J. Magn. Reson. 190 (2008) 307–315.

[33] M.K. Stehling, R. Turner, P. Mansfield, Echo-planar imaging: magnetic resonance imaging in a fraction of a second, Science 254 (1991) 43–50.

[34] F. Schmitt, M.K. Stehling, R. Turner, Echo-planar Imaging – Theory, Technique and Applications, Springer-Verlag, 1998.

[35] J. Granwehr, J.T. Urban, A.H. Trabesinger, A. Pines, NMR detection using laser-polarized xenon as a dipolar sensor, J. Magn. Reson. 176 (2005) 125–139.